

Self-Organized Time Crystal in Driven-Dissipative Quantum System

Ya-Xin Xiang,¹ Qun-Li Lei,¹ Zhengyang Bai,^{2,*} and Yu-Qiang Ma^{1,†}

¹National Laboratory of Solid State Microstructures and School of Physics,
Collaborative Innovation Center of Advanced Microstructures, Nanjing University, Nanjing 210093, China

²State Key Laboratory of Precision Spectroscopy,
East China Normal University, Shanghai 200062, China

Continuous time crystals (CTCs) are characterized by sustained oscillations that break the time translation symmetry. Since the ruling out of equilibrium CTCs by no-go theorems, the emergence of such dynamical phases has been observed in various driven-dissipative quantum platforms. The current understanding of CTCs is mainly based on mean-field (MF) theories, which fail to address the problem of whether the continuous time-translation symmetry can be broken in noisy, spatially extended systems absent in all-to-all couplings. Here, we propose a CTC realized in a quantum contact model through self-organized bistability (SOB). The CTCs stem from the interplay between collective dissipation induced by the first-order absorbing phase transitions (APTs) and slow constant driving provided by an incoherent pump. The stability of such oscillatory phases in finite dimensions under the action of intrinsic quantum fluctuations is scrutinized by the functional renormalization group method and numerical simulations. Occurring at the edge of quantum synchronization, the CTC phase exhibits an inherent period and amplitude with a coherence time linearly diverging with system size, thus also constituting a boundary time crystal (BTC). Our results serve as a solid route towards self-protected CTCs in strongly interacting open systems.

Introduction.—Time crystals are self-organized spatiotemporal structures, first envisaged by Wilczek [1, 2], that spontaneously break the time-translation symmetry imposed by underlying Hamiltonians. Since the advent of the no-go theorems stating that it is impossible to observe a spontaneously oscillating ground state (in thermal equilibrium)[3, 4], there have been several efforts concentrating on time crystals in closed Floquet systems [5–10]. Alternatively, coupling to an environment leads to the dissipative version of time crystals that break the discrete/continuous time-translation symmetry of the dynamical generators [11–19].

By building up a limit cycle (LC), the rise of synchronization in diverse physical platforms, such as optomechanical oscillators [20], Rydberg gases [21–23] and hybrid atom-cavity systems [24, 25], has been observed and related to the formation of CTCs. In open systems, the dissipation often associates with the quantum Langevin noise, it is probable that the fluctuations would affect the robustness of CTCs thereby destroying the crystalline order. Notwithstanding the rapid advances in experimental studies, to what extent the CTCs remain intact under the action of intrinsic noise is an open question worthy of theoretical endeavors.

Analogous to the famous notion of self-organized criticality (SOC), which is related to self-organization to the critical point of a continuous APT [26–33], the mechanism for SOB consists in a separation of the time scale of the dynamics of the order parameter from that of the corresponding control parameter. It triggers a LC phase of the hysteresis loop of a first-order APT [33, 34]. In light of the common features shared by LCs and CTCs, a new class of CTCs induced by SOB can be envisioned.

In this work, we theoretically investigate the formation and stability of CTCs beyond MF approximation. Con-

cretely, we consider a dissipative variant of the contact model characterized by the quantum and classical contact interactions between quantum emitters [35]. In the classical regime, the system undergoes continuous APTs. However, the transitions become discontinuous in the quantum regime. Upon addition of slow loading mechanism, a non-stationary phase arises from SOB, where the number of quantum emitters changes periodically [numerical results for three-dimensional systems sketched in Fig. 1(c)-(d)]. Meanwhile, the system undergoes repeated phase transitions and self-organizes to a CTC phase. Avalanches of activation, like fires spreading in a forest, trigger collective jumps from the absorbing to the active states, and terminate upon the exhaustion of emitters (trees), which in turn bring the system back into the absorbing state of slow recovery, waiting for the next jump. The CTC here is analogous to the breathing mode of “forest-fires” model [36]. Through theoretical analysis and numerical simulations, we find that the CTCs are unstable in low-dimensional systems, due to the reduced effective barrier separating the active from the absorbing states. Besides, our CTC suffers from phase noises caused by the kinetic trapping in absorbing state. Consequently, the coherence time diverges linearly with system size, whereas the degree of quantum synchronization decreases in larger systems.

Model.—Our model can be represented as an effective four-level system [Fig. 1(a)], where quantum emitters in active state $|a\rangle$ can spontaneously decay into the inactive state $|i\rangle$ (with rate Γ), and the inactive ones can be activated only in the vicinity of active ones both incoherently and coherently (with rates κ and Ω). Additionally, loss of emitters due to the decaying of active emitters into the removed states $|0\rangle$ (with rate $b\Gamma$), and an incoherent coupling $|p\rangle \rightarrow |i\rangle$ that mimics injecting inactive

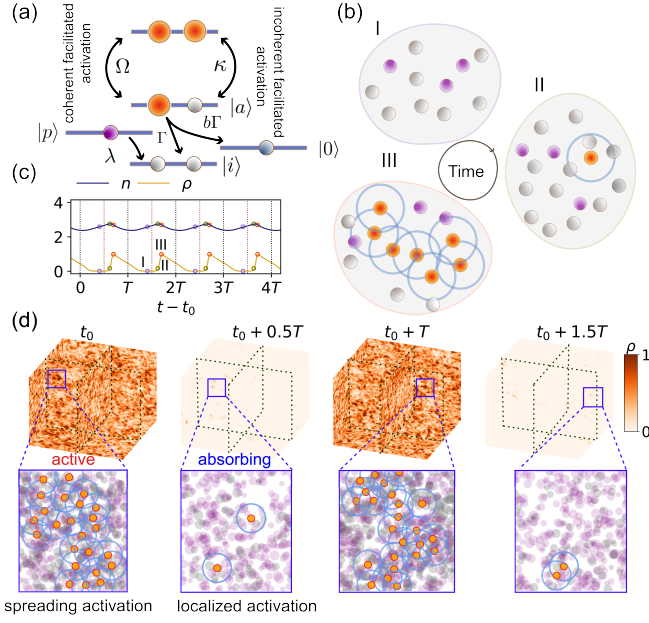


FIG. 1. (a) The effective four-level scheme. The quantum emitter in inactive state $|i\rangle$ (gray sphere) in proximity to emitters in active state $|a\rangle$ (red sphere) can become active via (in)coherent facilitated activation, and active emitters can spontaneously decay into either inactive or removed states $|0\rangle$ (blue sphere). Emitters in $|p\rangle$ state (purple sphere) are incoherently pumped to inactive state $|i\rangle$. (b) Sketch of CTC, where the contact activation occurs on the facilitation shell (large blue hollow sphere) of active emitters. The system typically consists of subcritical (I) and supercritical (II) states of low active densities, and supercritical highly active states (III). (c) Dynamical oscillations of the average total n and active ρ densities, corresponding to three states in panel (b). (d) Snapshots of the active density field from simulations are sketched.

emitters (with rate λ) are included. In free space, we can restrict the contact processes to pairs of emitters that are separated by the facilitation radius R_{fac} , and refer to the effective nearest neighbors of an active emitter as emitters at the border of its facilitation sphere [37].

Under the Markovian noise, the effective dynamics of this system permits a microscopic description for the density operator $\hat{\rho}$ via a Lindblad master equation $\partial_t \hat{\rho} = -i[\hat{H}, \hat{\rho}] + \sum_{\alpha} \mathcal{L}_{\alpha} \hat{\rho}$. The coherent activation is described by the effective Hamiltonian ($\hbar \equiv 1$ henceforth)

$$\hat{H} = \Omega \sum_l \hat{C}_l \hat{\sigma}_l^x, \quad (1)$$

where $\hat{C}_l = \sum_{k \in \partial l} \hat{\sigma}_k^{aa}$, $\hat{\sigma}_l^{\alpha\beta} \equiv |\alpha\rangle_l \langle \beta|_l$ ($\alpha, \beta = a, i, p, 0$), l, k are indices for each emitter, and $\sum_{k \in \partial l}$ denotes a summation of the effective nearest neighbors of the l -th emitter. The operator $\hat{\sigma}_l^x = \hat{\sigma}_l^- + \hat{\sigma}_l^+$ flips the quantum state with the ladder operators $\hat{\sigma}_l^+ \equiv \hat{\sigma}_l^{ai}$ and $\hat{\sigma}_l^- \equiv \hat{\sigma}_l^{ia}$.

The dissipative dynamics is described by Lindblad terms $\mathcal{L}_{\alpha} \hat{\rho} = \sum_l \left[\hat{L}_{\alpha, l} \hat{\rho} \hat{L}_{\alpha, l}^{\dagger} - \frac{1}{2} \left\{ \hat{L}_{\alpha, l}^{\dagger} \hat{L}_{\alpha, l}, \hat{\rho} \right\} \right]$. The

spontaneous inactivation of the active states is described by $\hat{L}_{d, l} = \sqrt{\Gamma} \hat{\sigma}_l^-$, and $\hat{L}_{p, l} = \sqrt{\gamma_{de}} \hat{\sigma}_l^{aa}$ represents dephasing of quantum coherence with rate γ_{de} . Meanwhile, the loss and reloading of inactive emitters are accounted for by $\hat{L}_{e, l} = \sqrt{b\Gamma} \hat{\sigma}_l^{0a}$ and $\hat{L}_{a, l} = \sqrt{\lambda} \hat{\sigma}_l^{ip}$, respectively. The incoherent contact processes are also included in Lindbladian, where the respective jump operators for activation and inactivation of emitters are given by $\hat{L}_{b, l} = \sqrt{\kappa} \hat{C}_l \hat{\sigma}_l^+$ and $\hat{L}_{c, l} = \sqrt{\kappa} \hat{C}_l \hat{\sigma}_l^-$.

The Heisenberg-Langevin equations of motion for the operators $\hat{\sigma}_l^{x/aa}$, $\hat{\sigma}_l^y = i\hat{\sigma}_l^- - i\hat{\sigma}_l^+$, and $\hat{n}_l = \hat{\sigma}_l^{aa} + \hat{\sigma}_l^{ii}$ read

$$\partial_t \hat{\sigma}_l^{aa} = -\Gamma \hat{\sigma}_l^{aa} + \Omega \hat{C}_l \hat{\sigma}_l^y + \kappa \hat{C}_l (\hat{n}_l - 2\hat{\sigma}_l^{aa}) + \hat{\xi}_l^{aa} \quad (2a)$$

$$\partial_t \hat{\sigma}_l^x = -\frac{\kappa \hat{N}_l + \gamma}{2} \hat{\sigma}_l^x - \kappa \hat{C}_l \hat{\sigma}_l^x - \Omega \hat{P}_l \hat{\sigma}_l^y + \hat{\xi}_l^x \quad (2b)$$

$$\partial_t \hat{\sigma}_l^y = -\frac{\kappa \hat{N}_l + \gamma}{2} \hat{\sigma}_l^y - \kappa \hat{C}_l \hat{\sigma}_l^y + \Omega \hat{P}_l \hat{\sigma}_l^x \quad (2c)$$

$$+ 2\Omega \hat{C}_l (\hat{n}_l - 2\hat{\sigma}_l^{aa}) + \hat{\xi}_l^y$$

$$\partial_t \hat{n}_l = -b\Gamma \hat{\sigma}_l^{aa} + \lambda \hat{\sigma}_l^{pp} + \hat{\xi}_l^n \quad (2d)$$

where $\hat{N}_l = \sum_{k \in \partial l} \hat{n}_k$, $\hat{P}_l = \sum_{k \in \partial l} \hat{\sigma}_k^x$, and $\gamma = \Gamma + \gamma_{de}$. The Langevin noise operators $\hat{\xi}_l^{x/y/aa/n}$ appear because the dissipation is attributed to the coupling between the system and a large reservoir [38], and can be fixed via solving the Heisenberg equations under the reservoir Hamiltonians in Born-Markov approximation [See Supplemental Material (SM) for details]. Thereafter, we set the time unit to $\Gamma^{-1} = 1$.

In the following, we consider the continuum limit and after coarse-graining transform the expectation values of the operators into classical fields. More specifically, the fields of active and total densities are defined as $\rho(\mathbf{r}, t) \equiv \langle \text{Tr} \{ \hat{\sigma}_l^{aa} \hat{\rho} \} \rangle_{\mathbf{r}}$ and $n(\mathbf{r}, t) \equiv \langle \text{Tr} \{ \hat{n}_l \hat{\rho} \} \rangle_{\mathbf{r}}$, respectively, where $\langle \dots \rangle_{\mathbf{r}}$ denotes an average over the facilitation sphere centered at \mathbf{r} , and $\sigma^{x/y}$ are defined similarly. Omitting the operator moments generated by the two-body interactions and perturbatively eliminating $\sigma^{x/y}$ via the Janssen-De Dominicis-Martin-Siggia-Rose procedure [39, 40] (see SM) lead to the following action for the active density field

$$S[\rho, \tilde{\rho}] = \int \tilde{\rho} \left[(\partial_t - D_{\rho} \nabla^2 + u_2) \rho + u_3 \rho^2 + u_4 \rho^3 - \frac{\mu}{2} \tilde{\rho} \right] \quad (3)$$

where $\tilde{\rho}$ is the Martin-Siggia-Rose auxiliary field related to the dynamic responses of ρ to perturbations, and $u_2 = 1 - n\kappa - 256n^2\Omega^4 / (n\kappa + \gamma)^7$, $u_3 = 2[\kappa - 2n\Omega^2 / (n\kappa + \gamma)]$, $u_4 = 8\Omega^2 / (n\kappa + \gamma)$, $\mu = (1 + n\kappa)\rho + 4n\Omega^2\rho^2 / (n\kappa + \gamma)^2$ are the coupling constants. The diffusion constant $D_{\rho} = D_{\text{T}} + n\kappa R_{\text{fac}}^2 / 2$, where D_{T} is the thermal diffusivity.

With the total density n conserved ($b, \lambda = 0$), the static phases are determined by the solutions to the saddle-point equations following variation of action (3) with

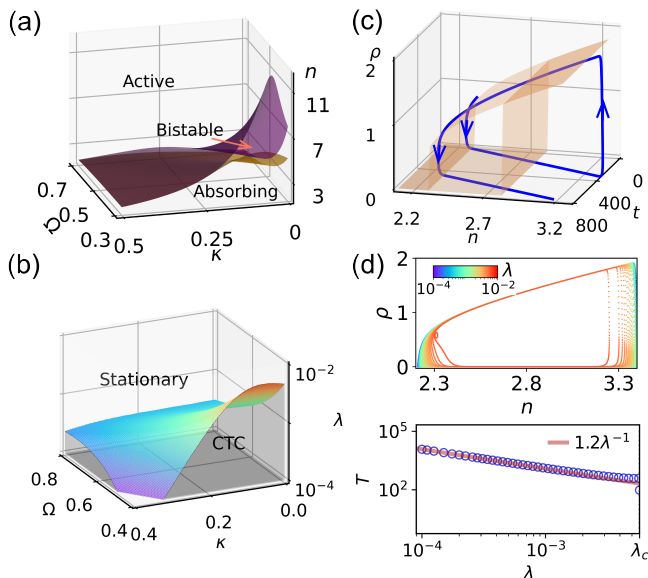


FIG. 2. Phase diagrams. (a) The two surfaces are the phase boundaries. Discontinuous APTs ensue when the two surfaces are separated from each other. (b) The surface represents the critical rate λ_c (color-coded) that separates a stationary phase from a CTC phase, corresponding to stable and unstable fixed points. (c) The CTC phase that consists of self-organized jumps (blue arrows) between the active and the absorbing phases (orange surfaces) for $\lambda = 3.2 \times 10^{-3}$. (d) Phase-space trajectories (upper) and periods (lower) as a function of λ .

$\tilde{\rho}, \tilde{n} = 0, D_T \rightarrow \infty$. The corresponding phase boundaries are shown in Fig. 2(a). In the quantum regime ($\Omega \gg \kappa$), the bistable region within the two boundaries indicates that the systems undergo discontinuous APTs when the total density n exceeds a critical value (see SM for relevant phase diagrams), which is an element of SOB-induced CTCs to be discussed later. Approaching the classical regime ($\Omega = 0$), the bistable region shrinks and finally vanishes when the transition becomes continuous, which has been related to SOC in driven-dissipative Rydberg gases [36, 37, 41].

SOB-induced CTCs.—Having identified the regime for first-order APTs, sustained oscillations can arise from the interplay between loss and reloading of emitters ($b, \lambda \neq 0$). Our proposal for SOB-induced CTCs is encoded in the Langevin equations for the density fields ρ, n as follows

$$\partial_t \rho = D_\rho \nabla^2 \rho + \tau n - u_2 \rho - u_3 \rho^2 - u_4 \rho^3 + \eta \quad (4a)$$

$$\partial_t n = D_T \nabla^2 n - b \rho + \lambda + \xi^n \quad (4b)$$

where η, ξ^n are Markovian white noises with vanishing mean and respective variance $\mu + \tau n$ and $b\rho$. To prevent the system from trapping in absorbing states, a small driving τn is added. Throughout the paper, we fix $\tau = 10^{-7}$, $b = 0.01$, $D_T = 1$, $n_p = 1$, $\kappa = 0$, $\Omega = 0.5$ and $\gamma = 2$, unless otherwise stated.

In the presence of first-order APTs [shaded region in Fig. 2(b)], one can identify a critical loading rate λ_c through a linear stability analysis of the fixed point possessed by Eqs. (4a) and (4b). The correlation functions diverge at a finite frequency, signaling the onset of broken time translation symmetry [42–44] [see SM]. The CTCs feature alternating jumps between the states with low and high active densities [Fig. 2(c)] with a period $\propto \lambda^{-1}$ [Fig. 2(d)]. The remaining is devoted to a systematic study of the CTC in finite systems.

Dimensionality dependence of CTC—We first discuss how dimensionality affects the stability of the CTCs. In lower dimensions, the effective barrier between the two states can be reduced. The jumps might occur at a wider range of total densities, thus destroying the long-range time crystalline order. To acquire a quantitative description, we adopt a functional renormalization group (fRG) approach via the Wetterich equation [45–47] to obtain the flows of the phase structure with decreasing infrared cutoff for various values of n in different dimensions (see SM). The resulting effective potential $\Phi_f(\rho)$ and the corresponding phase diagram are shown in Fig. 3. In $d = 1$, as n increases, the position of the local minimum shifts continuously from the origin to a finite value, indicating a continuous transition [Fig. 3(a)]. In $d \geq 2$, however, increasing n induces the appearance of a second local minimum at the finite density, apart from the local minimum at the origin, with a barrier in between, indicating a first-order transition [Fig. 3(b) and (c)]. Besides, the barrier is higher in $d = 3$ than $d = 2$, suggesting a weaker first-order transition in lower dimensions. The phase diagram in accord is shown in Fig. 3(d), where we can infer that discontinuous transitions are expected for $d \geq 2$. Compared with the MF results, the coexistence region

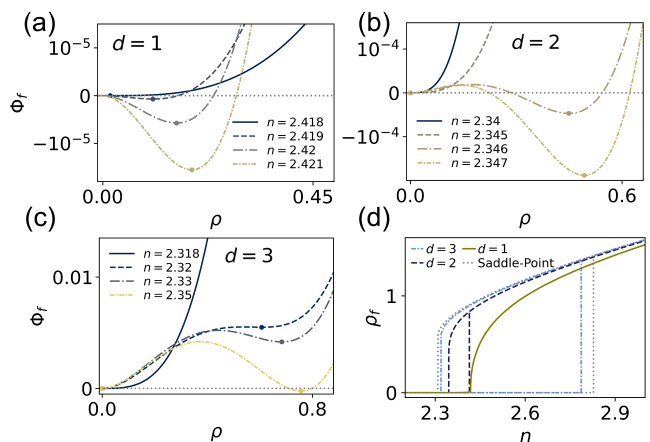


FIG. 3. The effective potential Φ_f as a function of the active density field ρ for different n in (a) $d = 1$, (b) $d = 2$, (c) $d = 3$. The active/absorbing phases are determined by the local minima (dots). (d) The corresponding phase diagram in comparison with that obtained via saddle-point approximation.

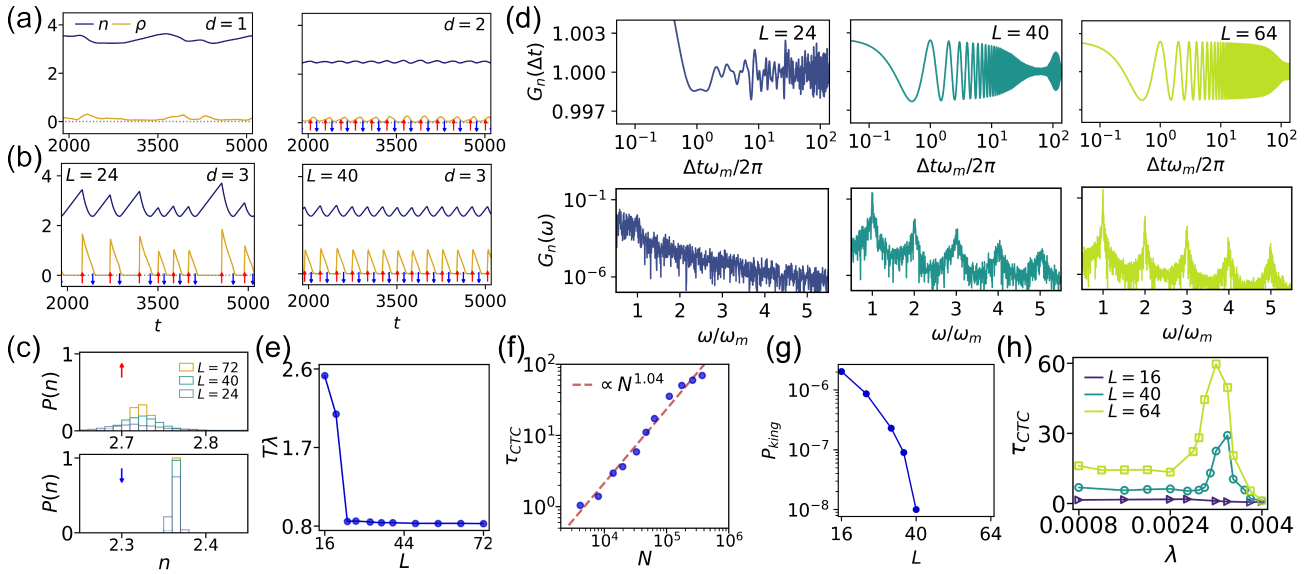


FIG. 4. Time series of the densities with collective jumps marked by red (blue) arrows in (a) low dimensions for $\lambda = 1.2 \times 10^{-3}$ with system size $L = 10^4$ (left), $L = 256$ (right) and (b) three-dimensional systems. (c) Probability distribution of the average total densities at which upward (upper) and downward (lower) jumps occur for varying L . (d) The autocorrelation functions $G_n(\Delta t)$ and their Fourier spectra $G_n(\omega)$, where the first peak ω_m dictates (e) the period $T = 2\pi/\omega_m$. (f) and (h) are the coherence time τ_{CTC} defined as the ratio of the period to its standard deviation, where $N = L^3$ is the system volume. (g) The occurrence probability of king avalanches. We select $d = 3$ [for (b)-(h)] and $\lambda = 3.2 \times 10^{-3}$ [for (b)-(g)].

becomes narrower for a lower dimensionality. The fRG results indicate that CTCs are possible in $d \geq 2$. The three-dimensional CTC is protected by a higher barrier and thus more stable.

We then numerically simulate Eqs. (4a) and (4b) deploying the operator-splitting scheme [48, 49], and record the time-series of the average densities, from which we detect collective quantum jumps. Deep in the CTC regime, oscillatory phases that entail a succession of periodic jumps are observed for $d = 2$ [Fig. 4(a), left panel]. Whereas compared with those in three-dimensional systems [Fig. 4(b), right panel], the jumps in two-dimensional occur on a much lesser scale, in accord with the much weaker first-order APTs therein, as revealed by the fRG analysis. Given the enhanced stability of CTCs in higher dimensionalities, in what follows, we restrict our discussion to $d = 3$. Results for $d = 1, 2$ are given in SM.

Finite-size effects.— As evinced in Fig. 4(b), more stable CTCs are expected in larger systems. Meanwhile, the distribution of average total density converges as the system is enlarged [Fig. 4(c)]. The two-time correlation functions $G_x(\Delta t) \equiv \langle x(t) \rangle_t^{-2} \langle x(t)x(t+\Delta t) \rangle_t$, for $x = n, \rho$ [22] manifest constant periodic oscillations for perfect time crystals[22]. Correspondingly, their Fourier spectra $G_x(\omega)$ peak at the integer multiples of their respective inherent frequencies ω_m . We can infer from Fig. 4(d), that in larger systems, the amplitude of $G_n(\Delta t)$ varies more slowly, and the Fourier spectra are more

sharply peaked at $\omega/\omega_m = 1, 2, 3, \dots$, typical of periodic structures in time. Besides, once the time crystalline order is built, the period $T \equiv 2\pi/\omega_m$ remains invariant with diverging L [Fig. 4(e)], and is thus inherent to CTCs. The existence of sustained oscillations with an intrinsic amplitude and frequency suggests that our CTCs are also a realization of BTCs [15].

Since upward jumps always lead to correlations among distant emitters (avalanches), the enhanced time crystallinity cannot be explained through the method of system-size expansion [14, 50–52]. The irregularity in the time series features a significant increase in the total density followed by an abrupt decrease in the active and total densities [see Fig. 4(b), left panel]. For low loading rates, such events have been attributed to the system falling into the absorbing state, and the consequent overloading in turn brings about system-spanning activation avalanches [53, 54]. For a three-dimensional CTC with a volume of $N = L^3$, the accumulated phase shift $\Delta\theta$ per cycle is approximately the probability of kinetic trapping in the absorbing phase $\sim 1/(TN\tau)$, and CTC should remain coherent over the time scale (rescaled by T) $\tau_{\text{CTC}} \approx 2\pi T/\Delta\theta$. We then estimates the coherence time from simulations by extracting the phase shifts via $\Delta\theta = 2\pi \langle \Delta T \rangle / T$, where $\langle \Delta T \rangle$ is the standard deviation of the period. Results are plotted in Fig 4(f), where the coherence time increases nearly linearly with the volume with a prefactor of $1.5(4) \times 10^{-4}$. It's easy to reconcile the finite correlations and diverging coherence time in

the $N \rightarrow \infty$ limit, because the absorbing state is devoid of fluctuations and has a lifetime inversely proportional to N .

Also, the next upward jump following the kinetic trapping is likely to trigger huge avalanches. To test this idea, we count space-time activation avalanches by connecting sites with active densities larger than a threshold (τ) as neighbors in the time-forward direction and grouping them into clusters. The occurrence probability of huge avalanches (king avalanches, defined as those containing more than half the total number of sites) decreases as the system becomes larger [Fig. 4(g)], in line with the longer coherence time [Fig. 4(f)]. A comparison of τ_{CTC} among various loading rates and system sizes is displayed in Fig. 4(h), the regime for CTCs indicated by the significantly increased coherence time lies between that for the aperiodic oscillations and the fluctuating uniform ones, and widens in larger systems.

Frequent huge avalanches induce coherent changes in active and total densities among a great many sites and thus reflect the underlying quantum synchrony at its highest level. However, a lack of synchrony results in stationary states with small fluctuations that conserve time-translation invariance. Sustained periodic oscillations reside in between the above two scenarios, where discontinuous phase transitions spontaneously generate finite-range correlations, which are enough to trigger coherence among local sites and yet unable to support a global synchronization in infinite systems. In other words, SOB-induced CTCs arise at the edge of quantum synchronization.

Conclusion and discussion.—In this work, we propose a mechanism to realize self-protected CTCs with diffusive couplings. Our analysis is not restricted to APTs, and can be generalized to other systems with bi-/multi-stability. Our CTCs can be interpreted as a BTC [15], where the reservoir plays the role analogous to the bulk Hamiltonian. The model here can be implemented with coherent laser-driven Rydberg atoms in anti-blockade regime, where the electronic ground (Rydberg) states can be mapped to the inactive (active) states [35, 37, 41]. The relative importance of the coherent and incoherent activation processes can be controlled by driven lasers.

Revealing how temporal organization arises from the SOB-induced bifurcation in quantum many-body systems, our study extends the dynamical phase diagram for both SOB and instability-related LCs [33, 55, 56]. Alongside the coherent-state path integral formalism for reaction-diffusion systems [57–59], the procedures facilitate studying real-world critical-like events [32, 53, 60–63] through controllable platforms.

This work is supported by the National Natural Science Foundation of China under Grants No. 11974175, No. 12247102 and No. 12274131. We are grateful to the High Performance Computing Center (HPCC) of Nanjing University for performing the numerical calculations

in this paper on its blade cluster system.

* zhybai@lps.ecnu.edu.cn

† myqiang@nju.edu.cn

- [1] F. Wilczek, *Phys. Rev. Lett.* **109**, 160401 (2012).
- [2] A. Shapere and F. Wilczek, *Phys. Rev. Lett.* **109**, 160402 (2012).
- [3] P. Bruno, *Phys. Rev. Lett.* **111**, 070402 (2013).
- [4] H. Watanabe and M. Oshikawa, *Phys. Rev. Lett.* **114**, 251603 (2015).
- [5] V. Khemani, A. Lazarides, R. Moessner, and S. L. Sondhi, *Phys. Rev. Lett.* **116**, 250401 (2016).
- [6] N. Y. Yao, A. C. Potter, I.-D. Potirniche, and A. Vishwanath, *Phys. Rev. Lett.* **118**, 030401 (2017).
- [7] S. Choi, J. Choi, R. Landig, G. Kucsko, H. Zhou, J. Isoya, F. Jelezko, S. Onoda, H. Sumiya, V. Khemani, C. von Keyserlingk, N. Y. Yao, E. Demler, and M. D. Lukin, *Nature* **543**, 221 (2017).
- [8] J. Smits, L. Liao, H. T. C. Stoof, and P. van der Straten, *Phys. Rev. Lett.* **121**, 185301 (2018).
- [9] F. M. Gambetta, F. Carollo, M. Marcuzzi, J. P. Garrahan, and I. Lesanovsky, *Phys. Rev. Lett.* **122**, 015701 (2019).
- [10] D. Bluvstein, A. Omran, H. Levine, A. Keesling, G. Semeghini, S. Ebadi, T. T. Wang, A. A. Michailidis, N. Maskara, W. W. Ho, S. Choi, M. Serbyn, M. Greiner, V. Vuletić, and M. D. Lukin, *Science* **371**, 1355 (2021).
- [11] H. Keßler, P. Kongkhambut, C. Georges, L. Mathey, J. G. Cosme, and A. Hemmerich, *Phys. Rev. Lett.* **127**, 043602 (2021).
- [12] S. Sarkar and Y. Dubi, *Communications Physics* **5**, 155 (2022).
- [13] F. Piazza and H. Ritsch, *Phys. Rev. Lett.* **115**, 163601 (2015).
- [14] C.-K. Chan, T. E. Lee, and S. Gopalakrishnan, *Phys. Rev. A* **91**, 051601 (2015).
- [15] F. Iemini, A. Russomanno, J. Keeling, M. Schirò, M. Dalmonte, and R. Fazio, *Phys. Rev. Lett.* **121**, 035301 (2018).
- [16] B. Buča, J. Tindall, and D. Jaksch, *Nat. Commun.* **10**, 1 (2019).
- [17] X. Nie and W. Zheng, *Phys. Rev. A* **107**, 033311 (2023).
- [18] Y. H. Chen and X. Zhang, *Nat. Commun.* **14**, 6161 (2023).
- [19] M. Krishna, P. Solanki, M. Hajdušek, and S. Vinjanampathy, *Phys. Rev. Lett.* **130**, 150401 (2023).
- [20] J. Sheng, X. Wei, C. Yang, and H. Wu, *Phys. Rev. Lett.* **124**, 053604 (2020).
- [21] D.-S. Ding, Z. Bai, Z.-K. Liu, B.-S. Shi, G.-C. Guo, W. Li, and C. S. Adams, *arXiv 2302.14145* (2023).
- [22] X. Wu, Z. Wang, F. Yang, R. Gao, C. Liang, M. K. Tey, X. Li, T. Pohl, and L. You, *arXiv:2305.20070* (2023).
- [23] K. Wadenpfuhl and C. S. Adams, *Phys. Rev. Lett.* **131**, 143002 (2023).
- [24] H. Keßler, J. G. Cosme, M. Hemmerling, L. Mathey, and A. Hemmerich, *Phys. Rev. A* **99**, 053605 (2019).
- [25] P. Kongkhambut, J. Skulte, L. Mathey, J. G. Cosme, A. Hemmerich, and H. Keßler, *Science* **377**, 670 (2022).
- [26] C. Tang and P. Bak, *J. Stat. Phys.* **51**, 797 (1988).
- [27] D. Sornette, *J. Phys. I* **2**, 2065 (1992).

- [28] M. Paczuski, S. Maslov, and P. Bak, *EPL* **27**, 97 (1994).
- [29] G. Grinstein, Generic scale invariance and self-organized criticality, in *Scale Invariance, Interfaces, and Non-Equilibrium Dynamics*, edited by A. McKane, M. Droz, J. Vannimenus, and D. Wolf (Springer US, Boston, MA, 1995) pp. 261–293.
- [30] L. Gil and D. Sornette, *Phys. Rev. Lett.* **76**, 3991 (1996).
- [31] R. Dickman, A. Vespignani, and S. Zapperi, *Phys. Rev. E* **57**, 5095 (1998).
- [32] R. Dickman, M. A. Muñoz, A. Vespignani, and S. Zapperi, *Braz. J. Phys.* **30**, 27 (2000).
- [33] V. Buendía, S. di Santo, J. A. Bonachela, and M. A. Muñoz, *Front. Phys.* **8**, 333 (2020).
- [34] S. di Santo, R. Burioni, A. Vezzani, and M. A. Muñoz, *Phys. Rev. Lett.* **116**, 240601 (2016).
- [35] M. Marcuzzi, M. Buchhold, S. Diehl, and I. Lesanovsky, *Phys. Rev. Lett.* **116**, 245701 (2016).
- [36] D.-S. Ding, H. Busche, B.-S. Shi, G.-C. Guo, and C. S. Adams, *Phys. Rev. X* **10**, 021023 (2020).
- [37] S. Helmrich, A. Arias, G. Lochead, T. M. Wintermantel, M. Buchhold, S. Diehl, and S. Whitlock, *Nature* **577**, 481 (2020).
- [38] L. Pan, X. Chen, Y. Chen, and H. Zhai, *Nat. Phys.* **16**, 767 (2020).
- [39] H.-K. Janssen, *Z. Physik B* **23**, 377 (1976).
- [40] P. C. Martin, E. D. Siggia, and H. A. Rose, *Phys. Rev. A* **8**, 423 (1973).
- [41] K. Klocke and M. Buchhold, *Phys. Rev. A* **99**, 053616 (2019).
- [42] T. E. Lee, H. Häffner, and M. C. Cross, *Phys. Rev. A* **84**, 031402 (2011).
- [43] O. Scarlatella, R. Fazio, and M. Schiró, *Physical Review B* **99**, 10.1103/PhysRevB.99.064511 (2019).
- [44] X. Nie and W. Zheng, *Physical Review A* **107**, 10.1103/PhysRevA.107.033311 (2023).
- [45] C. Wetterich, *Phys. Lett. B* **301**, 90 (1993).
- [46] L. Canet, H. Chaté, and B. Delamotte, *J. Phys. A: Math. Theor.* **44**, 495001 (2011).
- [47] N. Dupuis, L. Canet, A. Eichhorn, W. Metzner, J. Pawłowski, M. Tissier, and N. Wschebor, *Phys. Rep.* **910**, 1 (2021).
- [48] L. Pechenik and H. Levine, *Phys. Rev. E* **59**, 3893 (1999).
- [49] I. Dornic, H. Chaté, and M. A. Muñoz, *Phys. Rev. Lett.* **94**, 100601 (2005).
- [50] N. V. Kampen, *Stochastic Processes in Physics and Chemistry*, 3rd ed., North-Holland personal library (Elsevier, Singapore, 2007).
- [51] R. P. Boland, T. Galla, and A. J. McKane, *J. Stat. Mech.* **2008**, P09001 (2008).
- [52] A. Cabot, L. S. Muhle, F. Carollo, and I. Lesanovsky, *Phys. Rev. A* **108**, L041303 (2023).
- [53] P. Grassberger, *New J. Phys.* **4**, 17 (2002).
- [54] O. Kinouchi, L. Brochini, A. A. Costa, J. G. F. Campos, and M. Copelli, *Sci. Rep.* **9**, 3874 (2019).
- [55] I. R. Epstein and K. Showalter, *J. Phys. Chem.* **100**, 13132 (1996).
- [56] R. Lefever and G. Nicolis, *J. theor. Biol.* **30**, 267 (1971).
- [57] M. Doi, *J. Phys. A: Math. Gen.* **9**, 1479 (1976).
- [58] L. Peliti, *J. Physique* **46**, 1469 (1985).
- [59] K. J. Wiese, *Phys. Rev. E* **93**, 042117 (2016).
- [60] B. D. Malamud, G. Morein, and D. L. Turcotte, *Science* **281**, 1840 (1998).
- [61] N. Yoshioka, *Earth Planet. Sp.* **55**, 283 (2003).
- [62] J. M. Beggs and D. Plenz, *J Neurosci* **23**, 11167 (2003).
- [63] J. A. Bonachela and M. A. Muñoz, *J. Stat. Mech.* **2009**, P09009 (2009).